Anal. Chem. **2009,** *81,* 1496–1504

Quantitative Assessment of Hepatic Fat of Intact Liver Tissues with Coherent Anti-Stokes Raman Scattering Microscopy

Yao-Ming Wu,[†] Hung-Che Chen,[‡] Wei-Tien Chang,[†] Jhen-Wei Jhan,[‡] Hung-Lung Lin,[‡] and Ian Liau*[,‡]

National Taiwan University Hospital and College of Medicine, Taipei 100, Taiwan, and Department of Applied Chemistry and Institute of Molecular Science, National Chiao Tung University, Hsinchu 300, Taiwan

A fatty liver might progress from being a benign fatty liver, to steatohepatitis, cirrhosis, or even hepatocellular carcinoma. The great prevalence and severe outcome have warranted much investigation of the pathology and the development of effective therapies, which involve animal studies requiring critical evaluation of the hepatic fatty change. Histological examination and wet chemical analysis of liver biopsy specimens are generally employed for this purpose despite numerous procedures being involved. Using coherent anti-Stokes Raman scattering (CARS) microscopy, we have demonstrated the specific imaging of fat droplets in intact liver tissues and extracted the hepatic fat content through image analysis while eliminating laborious procedures required by traditional histopathological examination. The content of hepatic fat measured with CARS imaging was correlated strongly with that determined by biochemical analysis ($R^2 = 0.89$) over a pathologically significant range of the hepatic fat (from 2% to 20% of the total mass of tissue). Our work validates the quantitative assessment of fat in intact tissue through the use of CARS microscopy. When combined with the increasingly diverse animal models of diseases related to metabolic disorders of lipids, our approach is extensible to enable acquiring important insight into the genetic, environmental, and dietary factors affecting the uptake and accumulation of fat within tissues.

Hepatic steatosis, also known as fatty liver, is a common liver disease characterized by an excessive accumulation of triglyceride within hepatocytes (liver cells).[1] Factors including abuse of alcohol or drugs, starvation, obesity, resistance to insulin, and viral hepatitis have all been attributed to the pathogenesis of fatty liver.[2,3] In particular, nonalcoholic fatty liver disease (NAFLD), a manifestation of the metabolic syndrome of liver,[3] was reported to be the most prevalent liver disease and to affect one-fifth of the global adult population and up to two-thirds of obese individuals in affluent nations.[4] Moreover, fatty liver might progress to steatohepatitis, cirrhosis, and even hepatocellular carcinoma (liver cancer) in some proportion of individuals.[1] In view of its great prevalence and severe outcome, fatty liver diseases have over the past decade attracted much basic and clinical research effort.

A great majority of the research work on fatty liver diseases involve animal studies at some stages using rats or mice as a disease model. These animal studies usually require evaluation of the hepatic fatty change in a quantitative manner. The ability to quantify hepatic fat in these animal studies allows critical assessment to not only the progression of fatty liver in the disease model but also the efficacy of potential therapies against the disease. Although ultrasonography and computerized tomography have served as common medical-imaging tools to diagnose fatty liver for human beings,[5−8] they are less popular for studies on small animals such as rats. Furthermore, their signals are not based on chemically specific determinants, thereby allowing only qualitative assessment of hepatic fat. Although with proton magnetic resonance imaging or spectroscopy one can quantify gross hepatic fat with great specificity,[9,10] its great cost has been an obstacle for convenient access for researchers. Besides, none of the above medical-imaging tools possess sufficient spatial resolution and sensitivity to characterize hepatic fat droplets at the level of cells; this vital information is essential in studies of the uptake and accumulation of lipids by hepatocytes.[11,12] As a result, histological examination on liver tissues is routinely performed in animal studies of fatty liver diseases.

* To whom correspondence should be addressed. E-mail: ianliau@mail.nctu.edu.tw.

[†] National Taiwan University Hospital and College of Medicine.

[‡] National Chiao Tung University.

(1) Farrell, G. C.; Larter, C. Z. *Hepatology* **2006**, *43*, S99–S112.
(2) Angulo, P. *N. Engl. J. Med.* **2002**, *346*, 1221–1231.
(3) Neuschwander-Tetri, B. A. *Curr. Opin. Gastroenterol.* **2007**, *23*, 193–198.
(4) Marchesini, G.; Bugianesi, E.; Forlani, G.; Cerrelli, F.; Lenzi, M.; Manini, R.; Natale, S.; Vanni, E.; Villanova, N.; Melchionda, N.; Rizzetto, M. *Hepatology* **2003**, *37*, 917–923.
(5) Perez, N. E.; Siddiqui, F. A.; Mutchnick, M. G.; Dhar, R.; Tobi, M.; Ullah, N.; Saksouk, F. A.; Wheeler, D. E.; Ehrinpreis, M. N. *J. Clin. Gastroenterol.* **2007**, *41*, 624–629.
(6) Mishra, P.; Younossi, Z. *Am. J. Gastroenterol.* **2007**, *102*, 2716–2717.
(7) Park, S. H.; Kim, P. N.; Kim, K. W.; Lee, S. W.; Yoon, S. E.; Park, S. W.; Ha, H. K.; Lee, M. G.; Hwang, S.; Lee, S. G.; Yu, E. S.; Cho, E. Y. *Radiology* **2006**, *239*, 105–112.
(8) Lee, S. W.; Park, S. H.; Kim, K. W.; Choi, E. K.; Shin, Y. M.; Kim, P. N.; Lee, K. H.; Yu, E. S.; Hwang, S.; Lee, S. G. *Radiology* **2007**, *244*, 479–485.
(9) Cotler, S. J.; Guzman, G.; Layden-Almer, J.; Mazzone, T.; Layden, T. J.; Zhou, X. H. J. *J. Magn. Reson. Imaging* **2007**, *25*, 743–748.
(10) Westphalen, A. C. A.; Qayyum, A.; Yeh, B. M.; Merriman, R. B.; Lee, J. A.; Lamba, A.; Lu, Y.; Coakley, F. V. *Radiology* **2007**, *242*, 450–455.
(11) Hellerer, T.; Axang, C.; Brackmann, C.; Hillertz, P.; Pilon, M.; Enejder, A. *Proc. Natl. Acad. Sci. U.S.A.* **2007**, *104*, 14658–14663.
(12) Debarre, D.; Supatto, W.; Pena, A. M.; Fabre, A.; Tordjmann, T.; Combettes, L.; Schanne-Klein, M. C.; Beaurepaire, E. *Nat. Methods* **2006**, *3*, 47–53.

10.1021/ac8026838 CCC: $40.75
Published on Web 01/16/2009

For human beings, histological examination following liver biopsy is an indispensable diagnosis to distinguish patients at various stages of the fatty liver disease; various stages might yield varied prognoses and require varied management strategies. Histological examination also remains commonly employed before or during hepatic surgery, because even moderately fatty liver might significantly increase perioperative morbidity and mortality for both a living donor of a split liver and a recipient of a transplanted liver.[13,14] Further, differentiation of steatohepatitis from a benign fatty liver can only be achieved with histological examination of liver biopsy specimens. Despite these unique features, standard histopathological examination suffers from serious drawbacks. It involves numerous procedures of sample preparation including dehydration, fixation, staining, and sectioning and is laborious and time-consuming.

The development of multiphoton optical microscopy has yielded significant advances for nondestructive characterization of intact biological tissues in their native conditions.[15,16] In particular, two-photon excited fluorescence (TPEF)[17−20] and second-harmonic generation (SHG) microscopy[21−24] are the two techniques most widely employed for biomedical applications. In comparison with traditional histological examination, multiphoton microscopy possesses numerous attractive features such as three-dimensional optical sectioning, subcellular spatial resolution, deep penetration of thick specimens, and minimum destruction of samples.[25] Recently, another multiphoton microscopy technique, coherent anti-Stokes Raman scattering (CARS) microscopy, has been developed.[26−31] Similar to other multiphoton imaging modalities, CARS microscopy employs near-IR excitation that increases the penetration depth of a thick specimen and decreases the radiative damage to samples—two features that are particularly attractive for tissue imaging.[32,33] The CARS signal is notably intrinsic and specific to the vibration associated with a particular functional group such as CH_2; CARS images thereby possess chemical contrast while requiring no exogenous labeling. With CARS set resonant to the wavenumber of the stretching mode of CH_2, CARS microscopy has been demonstrated for chemical imaging of a bilayer of phospholipids that comprise long fatty chains with many CH_2 moieties.[34] A similar approach has been utilized to visualize intracellular lipid droplets in differentiated fibroblasts,[35,36] lipid storage in *Caenorhabditis elegans*,[11] myelin sheaths of nerve tissues,[37] subcutaneous fat in porcine skin,[38] and the lipid core of an atherosclerotic blood vessel.[39,40] Quantification of the hepatic fat content in intact liver tissues has not yet been reported. Using CARS microscopy, we investigated intact liver tissues obtained from rats in which was induced a fatty change in liver with diets deficient in methionine and choline (MCD). Our approach derives an advantage of CARS microscopy that allows fat-selective imaging based on an intrinsic signal of lipids with no stain, thereby eliminating laborious procedures required in a traditional histopathological examination. With an image-based analysis, we have also demonstrated a reagent-free quantification of the hepatic fat content in intact liver tissues.

MATERIALS AND METHODS

Animals and Feeding Protocols. Female Wistard rats (National Taiwan University College of Medicine, Laboratory Animal Center, Taiwan) were used for this work. During the first 6−8 weeks after birth (mass ~200 g), the rats were kept on standard rodent chow (Laboratory Rodent Diet 5001; LabDiet, Richmond, IN). The rats were then randomly assigned to a control group receiving normal rodent chow that comprises protein (23%), carbohydrate (56%), and fat (4.5%) or to an experimental group receiving a MCD diet (Baker Amino-Acid Diet lacking choline and methionine 578B; TestDiet, Richmond, IN). Elimination of methioline and choline in food results in impaired production of very low density lipoprotein (VLDL) that produces in turn an impaired secretion of triglyceride and an excessive accumulation of hepatic fat.[41,42] All animals had free access to food and drinking water throughout these tests and were maintained under a cycle with 12 h light, 12 h dark. The rats in the experimental group underwent laparotomy to remove the liver after they were fed with MCD diet for 1, 2, and 4 weeks, respectively. The control was sacrificed at the sixth week. The liver specimens were rinsed with normal saline solution and divided for separate assays as described below.

(13) Mortele, K. J.; Cantisani, V.; Troisi, R.; de Hemptinne, B.; Silverman, S. G. *Liver Transplant.* **2003**, *9*, S6–S14.
(14) Vetelainen, R.; van Vliet, A.; Gouma, D. J.; van Gulik, T. M. *Ann. Surg.* **2007**, *245*, 20–30.
(15) Zipfel, W. R.; Williams, R. M.; Webb, W. W. *Nat. Biotechnol.* **2003**, *21*, 1368–1376.
(16) Helmchen, F.; Denk, W. *Nat. Methods* **2005**, *2*, 932–940.
(17) Squirrell, J. M.; Wokosin, D. L.; White, J. G.; Bavister, B. D. *Nat. Biotechnol.* **1999**, *17*, 763–767.
(18) So, P. T. C.; Dong, C. Y.; Masters, B. R.; Berland, K. M. *Annu. Rev. Biomed. Eng.* **2000**, *2*, 399–429.
(19) van Zandvoort, M.; Engels, W.; Douma, K.; Beckers, L.; oude Egbrink, M.; Daemen, M.; Slaaf, D. W. *J. Vasc. Res.* **2004**, *41*, 54–63.
(20) Boulesteix, T.; Pena, A. M.; Pages, N.; Godeau, G.; Sauviat, M. P.; Beaurepaire, E.; Schanne-Klein, M. C. *Cytometry, Part A* **2006**, *69A*, 20–26.
(21) Campagnola, P. J.; Loew, L. M. *Nat. Biotechnol.* **2003**, *21*, 1356–1360.
(22) Brown, E.; McKee, T.; diTomaso, E.; Pluen, A.; Seed, B.; Boucher, Y.; Jain, R. K. *Nat. Med.* **2003**, *9*, 796–800.
(23) Fu, Y.; Wang, H. F.; Shi, R. Y.; Cheng, J. X. *Biophys. J.* **2007**, *92*, 3251–3259.
(24) Strupler, M.; Pena, A. M.; Hernest, M.; Tharaux, P. L.; Martin, J. L.; Beaurepaire, E.; Schanne-Klein, M. C. *Opt. Express* **2007**, *15*, 4054–4065.
(25) Denk, W.; Srtrickler, J. H.; Webb, W. W. *Science* **1990**, *248*, 73–76.
(26) Zumbusch, A.; Holtom, G. R.; Xie, X. S. *Phys. Rev. Lett.* **1999**, *82*, 4142–4145.
(27) Cheng, J. X.; Volkmer, A.; Book, L. D.; Xie, X. S. *J. Phys. Chem. B* **2001**, *105*, 1277–1280.
(28) Kee, T. W.; Cicerone, M. T. *Opt. Lett.* **2004**, *29*, 2701–2703.
(29) Volkmer, A. *J. Phys. D: Appl. Phys.* **2005**, *38*, R59–R81.
(30) Kano, H.; Hamaguchi, H. O. *Jpn. J. Appl. Phys., Part 1* **2007**, *46*, 6875–6877.
(31) Muller, M.; Zumbusch, A. *ChemPhysChem* **2007**, *8*, 2157–2170.
(32) Evans, C. L.; Potma, E. O.; Puoris'haag, M.; Cote, D.; Lin, C. P.; Xie, X. S. *Proc. Natl. Acad. Sci. U.S.A.* **2005**, *102*, 16807–16812.
(33) Fu, Y.; Wang, H. F.; Huff, T. B.; Shi, R.; Cheng, J. X. *J. Neurosci. Res.* **2007**, *85*, 2870–2881.
(34) Potma, E. O.; Xie, X. S. *ChemPhysChem* **2005**, *6*, 77–79.
(35) Nan, X. L.; Cheng, J. X.; Xie, X. S. *J. Lipid Res.* **2003**, *44*, 2202–2208.
(36) Nan, X. L.; Tonary, A. M.; Stolow, A.; Xie, X. S.; Pezacki, J. P. *ChemBioChem* **2006**, *7*, 1895–1897.
(37) Huff, T. B.; Cheng, J. X. *J. Microsc. (Oxford)* **2007**, *225*, 175–182.
(38) Jhan, J.-W.; Chang, W.-T.; Chen, H.-C.; Lee, Y.-T.; Chen, C.-H.; Liau, I. *Opt. Express* **2008**, *16*, 16431–16441.
(39) Wang, H. W.; Le, T. T.; Cheng, J. X. *Opt. Commun.* **2008**, *281*, 1813–1822.
(40) Chang, W. T.; Jhan, J. W.; Wu, Y. M.; Chen, H. C.; Liau, I. *Arterioscler., Thromb., Vasc. Biol.* **2008**, *28*, E115–E115.
(41) Koteish, A.; Diehl, A. M. *Semin. Liver Dis.* **2001**, *21*, 89–104.
(42) Rinella, M. E.; Green, R. M. *J. Hepatol.* **2004**, *40*, 47–51.

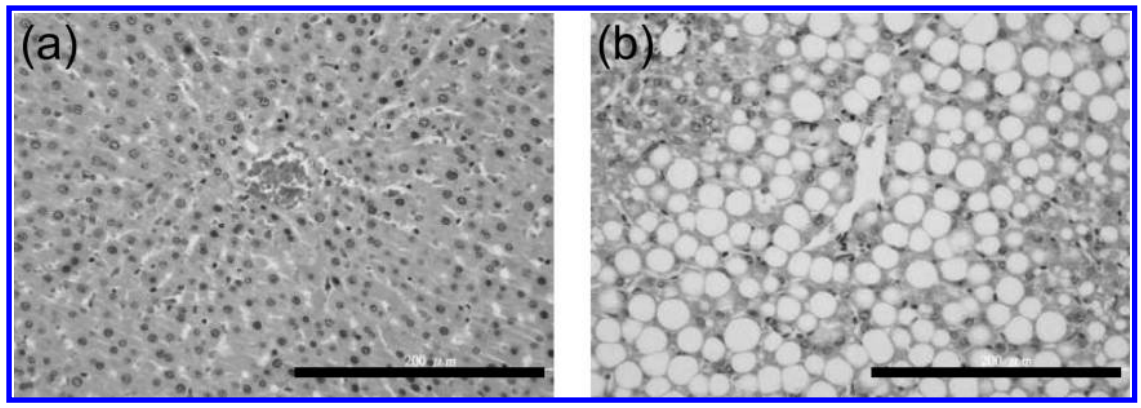

Figure 1. Micrographs of sections of liver specimens stained with hematoxylin and eosin (H/E) and taken from (a) a control and (b) an experimental group (fourth week). The observation of numerous large vacuoles in panel b indicates the accumulation of fat droplets in the rat liver and confirms that fatty liver has been induced by the MCD diet. Scale bar: 200 μm.

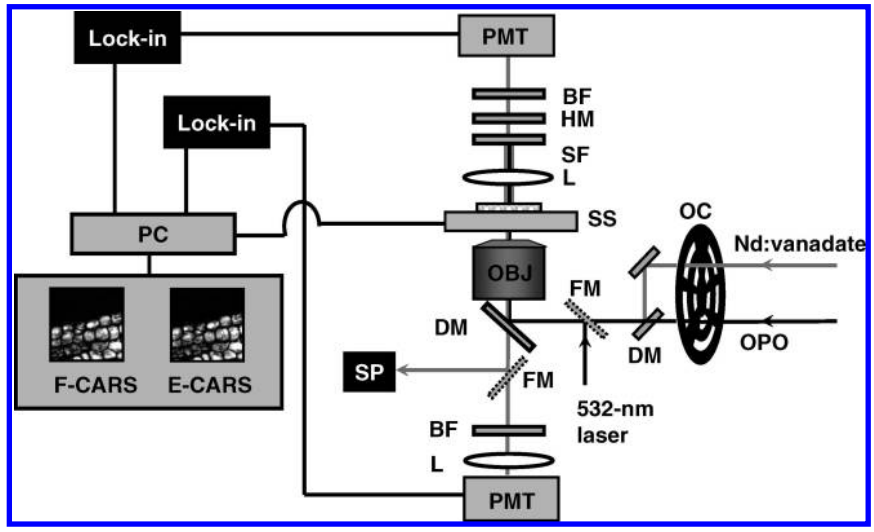

Figure 2. Schematic diagram of the CARS microscopy system employed to perform fat-specific imaging. OC denotes an optical chopper, Lock-in a lock-in amplifier, OBJ a microscope objective, PMT a photomultiplier sensor, SP a spectrograph, BF a band-pass filter, DM a dichroic mirror, FM a "flipper" mirror, HM a hot mirror, SF a short-pass filter, L a lens, and SS a scanning stage. Forward and backward CARS signals were collected simultaneously to produce images termed F-CARS and E-CARS, respectively.

For CARS imaging and Raman spectral characterization, a small piece of tissue (thickness about 1 mm) was excised from each lobe of liver, placed in a chambered coverslip, and immersed in normal saline solution with the liver capsule facing toward the microscope objective for en face characterization. All CARS images were obtained in a comparable depth, about 17 ± 2 μm from the capsule of the liver tissue, to ensure that all images were obtained from the outmost layer of hepatocytes.

Standard hematoxylin and eosin (H/E) stain was employed on sectioned liver tissue to confirm the results of introducing the MCD diet to rats. Bright-field images of H/E-stained specimens were recorded with an optical microscope equipped with a digital camera. Comparison of two images in Figure 1 confirms that fatty change was induced by the MCD diet. Fat-specific staining was employed using standard oil O red (ORO, Sigma-Aldrich, U.S.A.) stain. Two-photon excited fluorescence imaging was used to obtain fluorescence images of ORO-stained liver tissues.

All experimental protocols were approved by the National Taiwan University College of Medicine and College of Public Health Institutional Animal Care and Use Committee.

Confocal Raman Spectroscopy. Spontaneous Raman spectra of fat droplets in liver tissue were recorded using a home-built confocal Raman system. A diode-pumped solid-state laser (532 nm, DPSS-25; DPSS Lasers, U.S.A.) served for excitation. The laser beam was directed to the back port of an inverted microscope (IX71; Olympus, Japan) with a long-pass edge filter (LP03-532; Semrock, U.S.A.), and focused onto the sample with a microscope objective (UPLFLN 100×, N.A. 1.3; Olympus, Japan); the light scattered from the sample was collected with the same microscope objective. The edge filter allows the Stokes Raman scattering to pass while rejecting the Rayleigh scattering and the anti-Stokes Raman scattering. The Stokes scattering was then analyzed with a spectrograph (Shamrock 303; Andor, U.S.A.) equipped with a grating (600 groves/mm) and a thermoelectrically cooled CCD detector (iXon; Andor, England). The system was equipped also with a video camera and a manual stage to facilitate both the selection of areas of interest and the visualization of fat droplets. All spectra shown here have been subtracted from a baseline to remove the background and have been normalized. Polystyrene beads were used to optimize and to calibrate the system. The

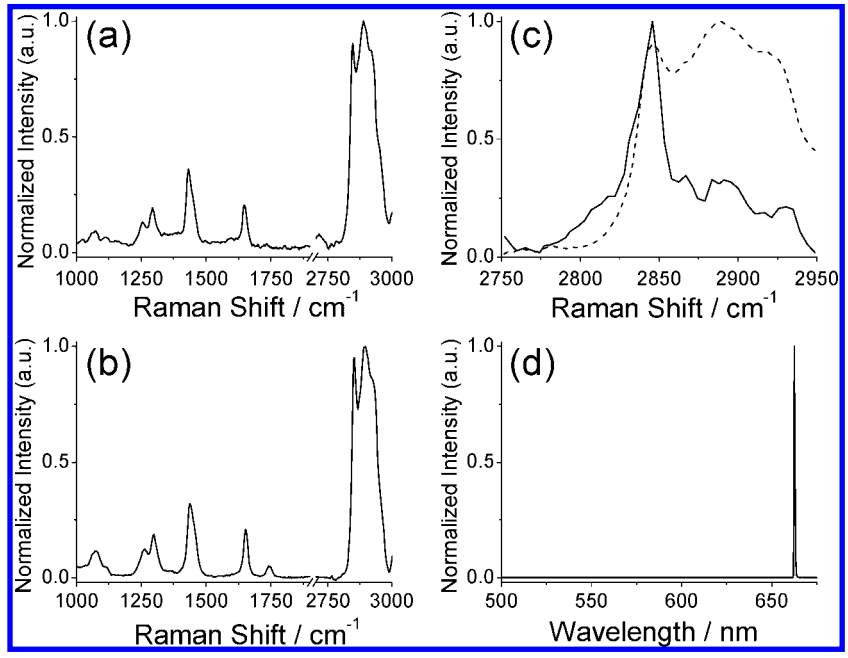

Figure 3. Results of spectral characterization of hepatic fat. Comparison of Raman spectra of a hepatic fat droplet (a) and that of adipocyte fat (b) indicates that hepatic fat is mainly triglyceride (excitation wavelength 532 nm, excitation power 20 mW; exposure duration of the spectrograph 20 s). (c) A CARS spectrum (solid line) measured on hepatic fat was employed to optimize the excitation wavelengths for CARS imaging of hepatic fat. The spontaneous Raman spectrum is shown as a dashed line. (d) The emission spectrum of CARS signals measured on hepatic fat on excitation at 816.7 and 1064 nm.

spectral resolution of the system was estimated to be 8 cm^{-1} from the full width at half-maximum (fwhm) of the Raman line of polystyrene at 1001 cm^{-1}.

CARS Microscopy, TPEF Microscopy, and CARS Spectroscopy. A schematic of the CARS microscope employed in this work appears in Figure 2. This microscope was modified from a system previously described;[38] only essential parts of the system are described here. A mode-locked Nd:vanadate laser (1064 nm, 7 ps, 76 MHz, PicoTran; High-Q Laser, Austria) and a synchronously pumped, optical parametric oscillator (OPO, tunable between 750 and 950 nm, Levante; APE, Germany) were employed as the "Stokes" and the "pump" excitations, respectively, to produce CARS. The two pulse trains were merged with a dichroic mirror, directed to an inverted optical microscope (IX71; Olympus, Japan), and focused onto the sample with a water-immersion objective (UPLSAPO 60×, N.A. 1.2; Olympus, Japan). For resonant imaging of fat, the wavelength of the "pump" excitation was tuned to 816.7 nm. The selection of the "pump" excitation in combination with Stokes excitation at 1064 nm produced a CARS signal associated with the CH_2 stretching mode with a Raman shift at 2850 cm^{-1}. For nonresonant imaging, the wavelength of the "pump" excitation was tuned to 862 nm corresponding to a Raman shift at 2202 cm^{-1}; this shift is located in the "silent" region of vibrational spectra and coincides with no vibrational wavenumber of common biological molecules. Forward- and backward-propagating CARS signals were collected simultaneously to produce F- and E-CARS images.[27] A phase-sensitive detection scheme was employed to increase the ratio of signal to noise.[38] The scanning of the sample was achieved with a three-axis, closed-loop piezo stage (P-563.3CD; Physik Instrumente, Germany). The images were constructed on recording signals point by point while raster-scanning the sample with respect to the fixed laser focal spot. The sample scanning, signal collection, and image construction were achieved with our own computer codes (LabView; National Instruments, U.S.A.).

For CARS spectral measurements, the intensity of the CARS signal was recorded as a function of the wavelength of the "pump" excitation that was tuned from 654 to 670 nm. The range corresponds to a Raman shift from 2750 to 2950 cm^{-1}. The spectrum was plotted with intensity of the signal as a function of the Raman shift.

For TPEF imaging of an ORO-stained specimen, we used the same system that served for CARS imaging except that only the 816.7 nm laser beam provided excitation, to produce TPEF of the ORO stain.

Biochemical Analysis of Triglyceride. A piece of liver tissue (mass about 100 mg) was excised from each lobe of liver and homogenized. The total lipid was extracted in a mixture (5 mL) of trichloromethane and methanol in proportion of 2:1 by volume. After being filtered to remove insoluble residues, the solution was maintained at 4 °C. The amounts of cholesterol and triglyceride were determined, in triplicate, using determination kits for cholesterol and triglyceride (Randox, U.K.). The concentration of fat is expressed as a mass fraction, corresponding to the number of milligrams of fat per gram of fresh liver tissue.

RESULTS AND DISCUSSION

Spectral Characterization of Hepatic Fat Droplets. To choose appropriate wavelengths for excitation with resonant CARS imaging of fat droplets, we first characterized fat droplets in liver tissues with their Raman spectra; Figure 3a shows a representative result. Several distinct lines observed in the fingerprint region are assigned to the C−C stretching mode (1070 cm^{-1}), the

C=C−H angular deformation (1259 cm^{-1}), the CH_2 bending mode (1300 cm^{-1}), the CH_2 twisting mode (1437 cm^{-1}), the C=C stretching mode (1659 cm^{-1}), and the C=O stretching mode (1740 cm^{-1}). An intense Raman feature comprising a superposition of multiple Raman lines between 2800 and 3000 cm^{-1} was also observed; these lines were associated with the stretching vibrations of CH_2 and CH_3 moieties. All these Raman lines are associated with vibrations characteristic of triglyceride molecules. In particular, the strong Raman line at 2846 cm^{-1} that corresponds to the symmetric stretching mode of CH_2 was observed, consistent with the abundance of CH_2 moieties in the long fatty chain of triglyceride.

The adipocyte fat in the subcutis of porcine skin comprises mainly triglyceride. To support our interpretation of the spectrum shown in Figure 3a, we measured the subcutaneous fat of porcine skin. A representative Raman spectrum of the subcutaneous fat is shown in Figure 3b; the positions of the Raman lines in the two spectra are strikingly similar. This observation strongly indicates that, similar to subcutaneous fat, the composition of hepatic fat comprises mainly triglyceride. As triglyceride molecules have abundant CH_2 moieties and as the CARS cross section for the CH_2 stretching mode is large, we chose resonant CARS corresponding to the wavenumber (2846 cm^{-1}) of the CH_2 stretching mode to produce fat-selective CARS images.

To optimize further the excitation wavelength for CARS imaging, we measured CARS spectra of hepatic fat according to a method described in the Materials and Methods section; the result appears in Figure 3c. The spectrum exhibits a line at 2846 cm^{-1}. For fat-selective CARS imaging the wavelengths of the "pump" and "probe" excitations were accordingly chosen to be 816.7 and 1064 nm, respectively. A representative spectrum of emission signals of hepatic fat with this setting is shown in Figure 3d. As expected, a single line located at 662.7 nm was observed confirming the generation of CARS.

CARS and Fluorescence Imaging of Fatty Liver Tissues. The results of our spectral characterization led to the "pump" and "Stokes" excitations selected at 816.7 and 1064 nm to yield images representing the distribution of CH_2 moieties, and thereby hepatic fat, according to our discussion. Figure 4a is an E-CARS image obtained on a liver specimen from a rat fed with the MCD diet for 4 days. We observed many small but bright spots prominent above the dark background resembling the fat vacuoles seen in the H/E stain image.

Both resonant and nonresonant CARS can contribute to the signal in the image shown in Figure 4a. To assess the relative contributions of resonant and nonresonant parts of CARS, we recorded a nonresonant CARS image in the same region according to methods described in the Materials and Methods section; the result is displayed in Figure 4b. The intensity of the image is in general small, and the image lacks appreciable contrast, indicating that the features seen in Figure 4a resulted mostly from the resonant CARS signal associated with CH_2 vibrations. As nonresonant CARS is independent of the wavelength of excitation, a minor nonresonant contribution of CARS to the image of Figure 4a can thus be estimated on integrating the pixel intensity of the nonresonant image; we return to this point later.

To confirm that the contrast seen in the CH_2-resonant CARS image is attributed to hepatic lipid droplets, we performed both CARS and TPEF imaging on an ORO-stained specimen. Parts c and d of Figure 4 illustrate the E-CARS and TPEF images obtained at the same region of an ORO-stained liver tissue. The two images exhibit similar contrast with almost all bright spots on the two images coincident with each other. This coincidence of bright spots on the CARS and ORO-stained TPEF images recorded at the same region unambiguously confirms that the contrast seen in Figure 4c, and thereby Figure 4a, represents the distribution of lipid droplets.

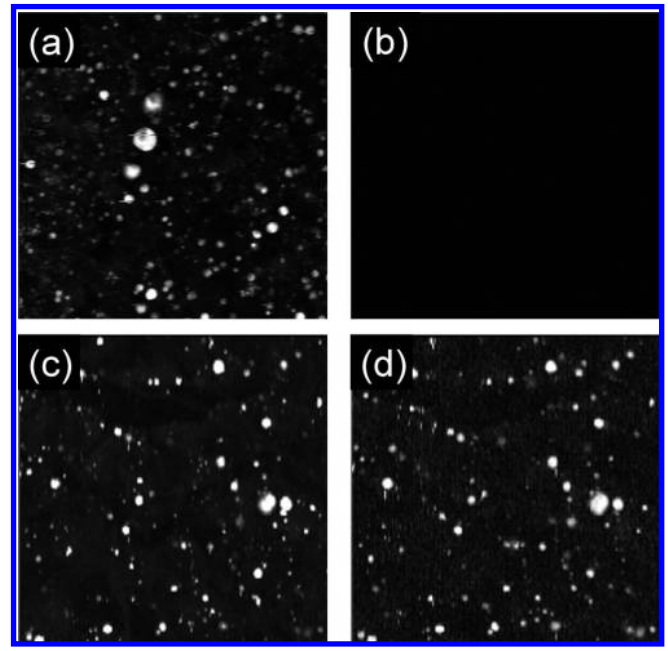

Figure 4. Resonant (a) and nonresonant (b) CARS images measured at the same region of an intact liver tissue. The specimen came from a rat that had developed mild fatty change after treatment of the MCD diet for 4 days. The nonresonant CARS image was obtained on setting the wavelength of the "pump" excitation at 862 nm, corresponding to a Raman shift 2202 cm^{-1}. The lack of contrast in the nonresonant image indicates that the contrast in panel a resulted mainly from the resonant contribution. A CARS image (c) and a fat-specific ORO-stained fluorescence image (d) were measured at the same region. The similar contrast and the coincidence of the bright spots observed in the two images confirm that the bright spots seen in CARS images represent hepatic fat. Scan area: 200 × 200 μm^2.

Progression of Hepatic Fatty Change Revealed by CARS Imaging. We conducted also a longitudinal test on rats with fatty liver to investigate the progression of fatty change in liver tissues; the method employed to induce fatty change of liver on rats is described in the Materials and Methods section.

Figure 5 shows E-CARS images recorded at the left, medial, and right lobes of liver tissues from the control and from the rats fed with the MCD diet for 1, 2, and 4 weeks. For the control, the intensity of the fat-selective CARS signal is slight, indicating an insignificant accumulation of hepatic fat for the rat fed with normal diet; this result is consistent also with few small vacuoles being observed in the H/E stain image of the control (Figure 1a). Some dim but large bright spots were observed in the CARS images obtained from the rat treated with the MCD diet for 1 week. Comparison of these images with that of the control exhibits notable differences among all three lobes of liver tissues. This result indicates that the onset of the fatty change is observable through CARS imaging as early as the first week of treatment

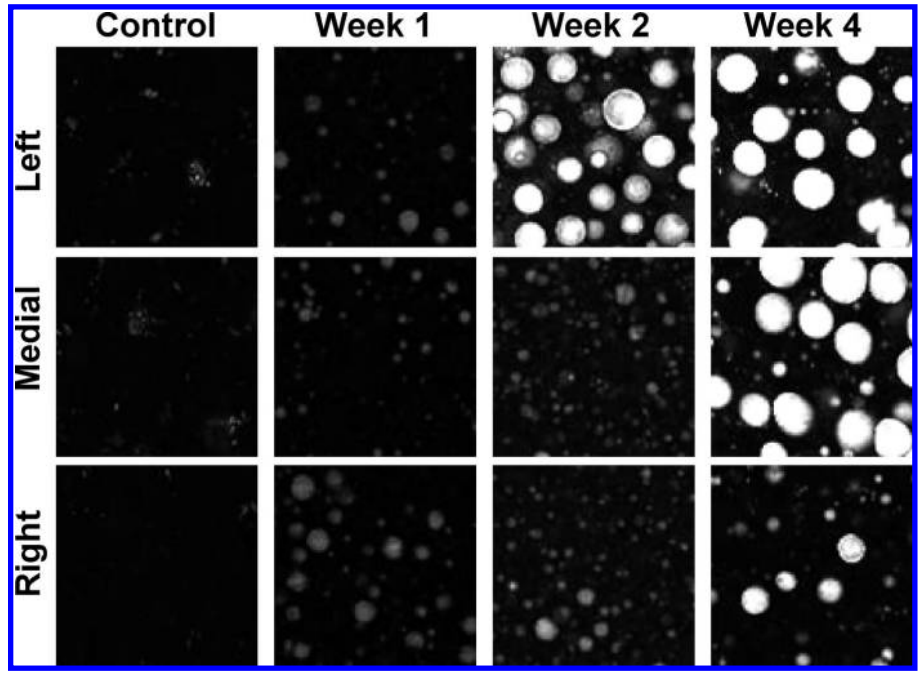

Figure 5. Fat-specific CARS images of the left, medial, and right lobes of liver specimens from a control group and an experimental group of rats treated with MCD diets for 1, 2, and 4 weeks. Scan area: 100 × 100 μm^2.

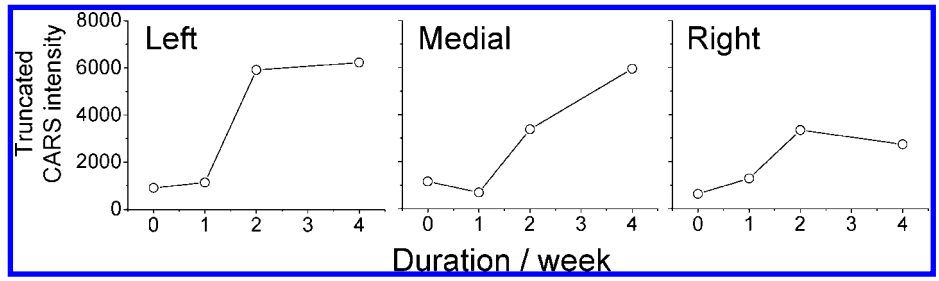

Figure 6. Truncated CARS intensities calculated from the fat-specific CARS images shown in Figure 5. Procedures to calculate the truncated CARS intensity are explained in the Materials and Methods section.

with the MCD diet. The number of large fat droplets detected by CARS imaging increased greatly with increasing duration of the MCD treatment. This trend is qualitatively consistent also with the results of histological examination on H/E-stained specimens that was performed in parallel with the CARS imaging as described in the Materials and Methods section (data not shown). The diameter of some fat droplets in the left lobe increased to about 25 μm in the second week, but the growth of these hepatic fat droplets seemed to attain a plateau with a similar size retained in the fourth week. The size of these fat droplets is almost comparable with that of the rat hepatocytes. These large droplets occupy a significant portion of space in the cytoplasm of hepatocytes and would inevitably perturb cellular activities resulting in impaired liver function.

We noticed also that the size and number of fat droplets observed in separate liver lobes of the same rat varied greatly. This heterogeneity among the three liver lobes might result from a variable uptake efficiency, metabolic activity, enzymatic kinetics, or circulation among these lobes. Elucidation of the underlying mechanism requires further investigations but is beyond the scope of the present work.

Image-Based Analysis of the Hepatic Fat Content. We have employed an image-based method to extract the hepatic fat content on analyzing the images. To validate our approach, the fat content extracted from the image analysis is compared with that determined from standard biochemical analysis.

The CARS signal arises from the third-order susceptibility, $\chi^{(3)}$, of a material that includes a resonant term, $\chi_r^{(3)}$, and a nonresonant term, $\chi_{nr}^{(3)}$. For the simplest situation in which all oscillators are identical, the intensity of the CARS signal produced from a group of identical oscillators is expressed as

$$I_{CARS} \propto |\chi^{(3)}|^2 = (\chi_r^{(3)} + \chi_{nr}^{(3)})^2 = \frac{n^2A^2}{\delta^2+\Gamma^2} + \frac{2nA\chi_{nr}^{(3)}}{\delta^2+\Gamma^2}\delta + (\chi_{nr}^{(3)})^2$$

in which appear symbols n for the number of oscillators, A for the Raman scattering strength of an oscillator, Γ for the fwhm of a Raman line associated with an oscillator; δ denotes the detuning defined as $\Omega - (\omega_P - \omega_{PR})$ with Ω as resonance wavenumber of the oscillator and ω_P and ω_{PR} as wavenumbers of the "pump"

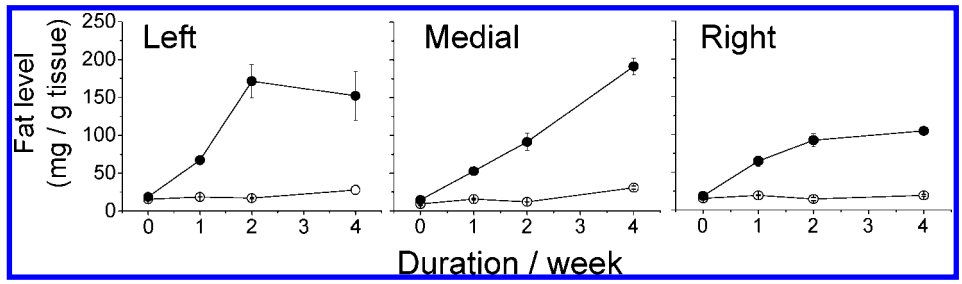

Figure 7. Content of triglyceride (solid circles) and cholesterol (empty circles) determined on the same liver specimens used for CARS imaging. The data points and the error bars represent the mean and standard deviations calculated from results of three repeated measurements.

and "probe" excitations, respectively. The contribution of the observed CARS signals is accordingly divided into three terms, the contributions of which are discussed later.

The relative contribution of the quadratic and the liner terms to the CARS signal can be examined by considering the ratio of the two terms which is expressed as

$$I_{n^2}/I_n = \left(\frac{n^2A^2}{\delta^2+\Gamma^2}\right)\Big/\left(\frac{2nA\chi_{\mathrm{nr}}^{(3)}}{\delta^2+\Gamma^2}\,\delta\right) = \frac{nA}{2\chi_{\mathrm{nr}}\delta}$$

Hepatic fat droplets are closely packed with triglyceride molecules, and each triglyceride has three long fatty chains with many CH_2 moieties in the C−C skeleton. In addition, the excitation zone created by our tightly focused laser has a size of order of 1 μm. As a result, the number of oscillators (i.e., the CH_2 moiety) probed with the laser excitation is very large ($n \gg 1$). Furthermore, since all the images in this work were obtained under a near-resonant condition, the detuning, δ, is thereby close to 0. The remaining parameter $(A)/(2\chi_{\mathrm{nr}})$ has been determined to be on the order of 1 for lipid molecules.[43] Taking these conditions into account, we reasonably assume that

$$I_{n^2}/I_n = \frac{nA}{2\chi_{\mathrm{nr}}\delta} \gg 1$$

We thus conclude that the contribution from the linear term is negligible in comparison to that from the quadratic term. The expression for the CARS intensity becomes simplified to

$$I_{\mathrm{CARS}} \propto n^2\left(\frac{A^2}{\delta^2+\Gamma^2}\right) + (\chi_{\mathrm{nr}}^{(3)})^2 \propto n^2\left(\frac{A^2}{\delta^2+\Gamma^2}\right) + I_{\mathrm{background}}$$

in which the expression has been rearranged slightly to feature the squared dependence of the CARS intensity on n. The term $(\chi_{\mathrm{nr}}^{(3)})^2$ is expressed as $I_{\mathrm{background}}$ because it contributes a background to the CARS image. As discussed earlier, this background contribution is independent of excitation wavelength and can be determined experimentally from a measurement performed under a nonresonant condition.

We derive this formula

$$I_{\mathrm{background-subtracted}} \propto n^2\left(\frac{A^2}{\delta^2+\Gamma^2}\right)$$

that implies the background-subtracted CARS intensity to be quadratically proportional to the number of oscillators as long as n is large. As triglyceride is the dominant component of hepatic fat, this fat content thus becomes represented as the amount of triglyceride molecules, which is, in turn, represented by the quantity of CH_2 oscillators, n_{CH_2}. The proportion of hepatic fat becomes thus experimentally determined from the square root of the image intensity in a background-subtracted CARS image:

$$\text{hepatic fat content} \propto n_{\mathrm{Triglyceride}} \propto n_{\mathrm{CH_2}} \propto \sqrt{I_{\mathrm{resonant}} - I_{\mathrm{nonresonant}}}$$

in which I_{resonant} and $I_{\mathrm{nonresonant}}$ are determined on calculating the summation of the intensity of pixels for images recorded under resonant and nonresonant conditions, respectively. Similar conclusions have also been suggested by others to approximate the relative concentration of oscillators by taking a square root of the CARS intensity.[44,45] This image-based method was employed to analyze the fat-selective images obtained from CARS imaging of the intact liver tissues. The result is summarized in the scatter plots in Figure 6, in which the truncated CARS intensity that represents the hepatic fat content, as discussed above, is plotted as a function of duration of feeding of rats with the MCD diet.

Correlation between Results from CARS Imaging and Wet Chemistry. A criterion to evaluate the validity of a proposed analytical method is to examine the correlation between results obtained with that method and a conventional method. To determine the fat level in tissue extracts, measurements from wet chemistry constitute such a generally accepted method, i.e., a standard. To establish a correlation between these methods, we employed wet chemical analysis in parallel with CARS imaging on each lobe of rat livers. Figure 7 shows the mean and standard deviation of the triglyceride and cholesterol level, obtained from triplicate measurements, plotted against duration of feeding of rats with the MCD diet. For the normal control, the triglyceride content is between 14.4 and 18.6 mg/g of tissue or slightly less than 2% of the tissue mass. The cholesterol level comparably ranges from 9 to 15 mg/g of tissue. In general, the triglyceride level increases with an increased duration of feeding rats with the MCD diet. The value continued to increase to 191 mg/g of tissue (19% of the tissue mass) for a lobe at the fourth week of MCD treatment. In contrast, the cholesterol level remained

(43) Cheng, J. X.; Volkmer, A.; Book, L. D.; Xie, X. S. *J. Phys. Chem. B* **2002**, *106*, 8493–8498.
(44) Cheng, J. X.; Volkmer, A.; Xie, X. S. *J. Opt. Soc. Am. B* **2002**, *19*, 1363–1375.
(45) Potma, E. O.; Xie, X. S.; Muntean, L.; Preusser, J.; Jones, D.; Ye, J.; Leone, S. R.; Hinsberg, W. D.; Schade, W. *J. Phys. Chem. B* **2004**, *108*, 1296–1301.

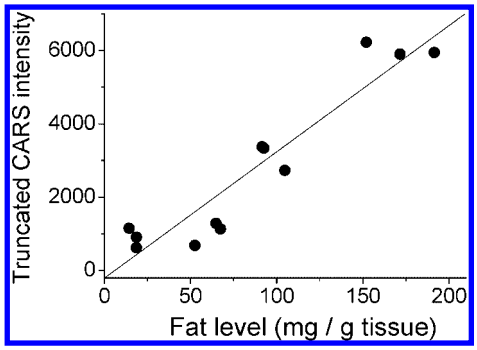

Figure 8. Scattered data show the correlation between the fat content determined from CARS imaging and from biochemical analysis. The solid line results from linear regression of these data points. $R^2 = 0.8901$ and $p < 0.001$.

unaltered as opposed to the triglyceride level, indicating that triglyceride dominates the hepatic fat in a fatty liver. The fat content determined from an individual liver lobe of a rat varies significantly, and a similar heterogeneity from lobe to lobe is observed in the fat-selective CARS images shown in Figure 5.

We obtained a correlation curve on plotting the hepatic fat content determined by CARS imaging against that determined from the standard wet chemical method; the result appears in Figure 8. The correlation coefficient, R^2, of a linear fit of this data set is 0.89, indicating a strong correlation. A main focus of this work is validation of the quantification of the hepatic fat level with CARS imaging, for which a correlation coefficient alone provides an essential measure. As a result, a strong correlation between data obtained from CARS imaging and biochemical analysis indicates our approach to be a promising method for determination of the hepatic fat content in intact liver tissue.

Another critical measure of an analytical method is an appropriate range of measurements. The data set shown in Figure 8 exhibits a close correlation up to 191 mg of the hepatic fat, equivalent to approximately 20% in terms of the tissue mass. The diagnosis of fatty liver is made when the fat content exceeds 5−10% by weight. Our result suggests that CARS microscopy possesses a sufficiently large dynamic range to distinguish between a normal and diseased liver with fatty change.

The same methodology of validation has also been employed to examine and validate the use of proton magnetic resonance spectroscopy (p-MRS) for the quantification of the hepatic fat content.[46] In that study, the correlation coefficient (R^2) was reported to be 0.87 and the hepatic fat content was determined up to 44.9 μmol/g of tissue (equivalent to 36 mg/g of tissue assuming the molecular weight of triglyceride is 799 g/mol). In comparison, the correlation coefficient obtained in our work is slightly better (0.89 vs 0.87) while the range of quantification is significantly improved (up to 190 mg/g of tissue vs 36 mg/g of tissue). The latter is of great clinical significance as it suggests that the quantification of fat with CARS microscopy possesses a sufficiently large dynamic range to characterize the progression of a fatty liver disease from a benign to a severe pathological condition.

For clinical measurements, an uncertainty as high as 20% is not unusual and is generally considered acceptable. The relatively uncertainty determined from the work using p-MRS is ±29% as estimated from the reported hepatic fat content of 44.9 ± 13.2 μmol/g of tissue.[46] From the result shown in Figure 8, the absolute uncertainty of our work at the medial value of the diagnostic criterion (i.e., 75 mg/g of tissue) is estimated to be ±10 mg/g of tissue, yielding a relative uncertainty of ±13.3%. Again, a significant improvement in the accuracy of quantification is obtained with CARS microscopy as shown from a reduced uncertainty (±13.3% vs 29%).

In principle, CARS is specific to only a particular resonant wavenumber associated with a functional group rather than being specific to a molecule of a particular kind. Disparate molecules carrying the same functional group, such as CH_2, might hence all contribute to a CARS signal detected in this work, which raises a concern for the application of CARS imaging to quantify fat because significant biomolecules such as proteins, carbohydrates, DNA, and phospholipids all contain similar functional groups, e.g., CH_2 moieties. We nevertheless contend that the CARS signal observed from the liver tissue was dominated by the CH_2 moieties in triglyceride fat. According to the results in Figure 7, hepatic fat comprises mainly triglyceride, especially for liver with severe fatty change. As hepatic fat droplets are closely packed with triglyceride molecules and as each triglyceride molecule has many CH_2 moieties, the number density of CH_2 moieties within a fat droplet is expected to be large. We assume that the number density of CH_2 moieties in the cytoplasm or in the extracellular matrix would be much less than that in a hepatic fat droplet, thereby contributing insignificantly to the detected under our experimental conditions. The quadratic dependence of the CARS signal on the number of oscillators magnifies the distinction between contributions from hepatic fat and other molecules. The coincidence of bright spots in Figure 4, parts c and d, taken at the same region, provides compelling evidence for this argument. We thus conclude that CARS imaging allows selective visualization of fat droplets in intact liver tissues and that the fat content can be extracted from the fat-selective CARS images.

Although the current study is employed on tissue explant, the unique capability of CARS microscopy for the visualization of fat droplets and the quantification of hepatic fat in intact tissues may enable applications in clinical settings. Since even moderately fatty liver might significantly increase perioperative morbidity and mortality for both a living donor of a split liver and a recipient of a transplanted liver, intraoperative examination with ultrasonography remains commonly employed during hepatic surgery such as liver transplantation. However, ultrasonography is unable to quantify fat. Its spatial resolution is also too crude to resolve fat droplets. By integrating with technology such as video-scanning,[32] fiber-optics,[47] robot systems, and imaging processing, we anticipate that CARS microscopy could also be further developed as an intravital-imaging modality for real-time visualization and quantification of hepatic fat during hepatic surgeries.

We have demonstrated an unprecedented capability of CARS imaging in the visualization of hepatic fat droplets and in the

(46) Szczepaniak, L. S.; Babcock, E. E.; Schick, F.; Dobbins, R. L.; Garg, A.; Burns, D. K.; McGarry, J. D.; Stein, D. T. *Am. J. Physiol.: Endocrinol. Metab.* **1999**, *276*, 977–989.

(47) Légaré, F.; Evans, C. L.; Ganikhanov, F.; Xie, S. X. *Opt. Express* **2006**, *14*, 4427–4432.

(48) Parekh, S.; Anania, F. A. *Gastroenterology* **2007**, *132*, 2191–2207.

quantification of the hepatic fat content in intact liver tissue. The findings cannot only be utilized to monitor the progression of diseases but also to facilitate the development of new therapies that employ animal studies. In addition, the results could help in the interpretation of results obtained from other medical-imaging modalities. Further, this approach is specifically extensible readily to quantify fat in various tissues. In view of increasingly numerous diseases related to the disorder of fat metabolisms,[48] this is of great clinical significance. When combined with the increasingly diverse animal models of diseases related to metabolic disorders of lipids, our technique should find widespread applications as an investigative tool that may lead to important insight into genetic, environmental, and dietary factors affecting the deposition and accumulation of fat within tissues.

CONCLUSION

We have demonstrated the quantification of hepatic fat in intact liver tissue using CARS microscopy. Our results show that CARS microscopy possesses sufficient sensitivity and an appropriate dynamic range for the determination of fatty change in liver at various stages of progression.

ACKNOWLEDGMENT

We thank Professors Yuan-Pern Lee, Kien-Wen Sun, Jeng-Tzong Sheu (NCTU), and Chung-Hsuan Chen (GRC, Academia Sinica) for the use of their equipment and Yi-Cyun Yang and Yu-Tsung Lee (NCTU) for technical assistance. We are also grateful to Professor John Ogilvie for comments on the manuscript. The National Science Council and the MOE−ATU program of Taiwan provided support to I.L.

Received for review September 23, 2008. Accepted December 27, 2008.

AC8026838